Available online at BCREC website: https://bcrec.id

Bulletin of Chemical Reaction Engineering & Catalysis, 18 (1) 2023, 151-161

Research Article

Investigate the Function and Structure of (Fe,Cr) $La_2Ti_2O_7$ Photocatalyst Calcined under the Nitrogen Atmosphere

Hussanai Luangthanarak[1], Ratchadaporn Supruangnet[2], Waraporn Tanthanuch[2,], Sukasem Watcharamaisakul[1,*]**

[1]*School of Ceramic Engineering, Institute of Engineering, Suranaree University of Technology, Nakhon Ratchasima, Thailand.*
[2]*Synchrotron Light Research Institute (Public organization), Nakhon Ratchasima, Thailand.*

Received: 11th March 2023; Revised: 8th April 2023; Accepted: 12th April 2023
Available online: 16th April 2023; Published regularly: April 2023

Abstract

Extensive research has been conducted on enhancing the photocatalytic activity of Lanthanum titanium oxide ($La_2Ti_2O_7$) based photocatalysts. However, these photocatalysts were found to be inactive under visible light. To address this limitation, a modification was developed by co-doping Fe and Cr on $La_2Ti_2O_7$ to enable visible light driven photocatalytic response. The calcination of (Fe,Cr) $La_2Ti_2O_7$ was carried out under nitrogen atmosphere at various temperatures for 24 h. The results showed that the (Fe,Cr)-$La_2Ti_2O_7$ calcined at 1250 °C for 24 h exhibited the highest methylene blue degradation under visible light. Synchrotron X-ray absorption spectroscopy indicated that Fe and Cr were substitutionally located adjacent to the Ti atom within the $La_2Ti_2O_7$ structure. This metal substitutionally facilitated electron transfer and perturbed the *p-d* hybridization by modifying the local electronic structure of the surrounding oxygen atoms and transition metal ions, thereby reducing the band gap energy and enhancing the photocatalytic capability.

Keywords: Photocatalyst; $La_2Ti_2O_7$; (Fe,Cr) co-doping; Nitrogen atmosphere; XAS; Synchrotron

How to Cite: H. Luangthanarak, R. Supruangnet, W. Tanthanuch, S. Watcharamaisakul (2023). Investigate the Function and Structure of (Fe,Cr) $La_2Ti_2O_7$ Photocatalyst Calcined under the Nitrogen Atmosphere. *Bulletin of Chemical Reaction Engineering & Catalysis*, 18(1), 151-161 (doi: 10.9767/bcrec.17634)

Permalink/DOI: https://doi.org/10.9767/bcrec.17634

1. Introduction

The use of photocatalysts in various applications related to the environment and energy has been widely researched for decades due to its prominent property of photocatalytic activity [1]. The number of publications in this field continues to rise each year, with over 1000 peer-reviewed publications per year. One of the main areas of focus in renewable and sustainable energy is solar energy, which relies on the photocatalytic process for efficient conversion [2,3]. Typically, photocatalytic efficiency is active under Ultraviolet (UV) region due the high energy in this region can excite electrons from the valence band to the conduction band, which initiates a redox reaction. The excited electrons (e^-_{CB}) in the conduction band react with oxygen (O_2), for the valence band has left the positive holes (h^+_{VB}) obtaining water oxidation as the formation of active species: hydroxyl radical ($OH^\bullet$), hydrogen peroxide, superoxide ($O_2^{-\bullet}$), *etc.* [4–7]. The layered perovskite structure, which has a general formula of $A_2B_2O_7$, possesses a unique electronic configuration that allows

Corresponding Author.
*Email: sukasem@sut.ac.th (S. Watcharamaisakul);
**Email: waraporn@slri.or.th (W. Tanthanuch);

it to exhibit photocatalytic performance when highly donor-doped. This structure is also highly stable and can participate in redox reactions. One notable member of this structure is $La_2Ti_2O_7$, which has demonstrated high efficiency in photocatalytic water splitting to produce H_2 and O_2. Furthermore, various applications of $La_2Ti_2O_7$ are used: decomposed isopropyl alcohol, decomposition of harmful organics, evolution of H_2 from water-ethanol solution, *etc*. Moreover, $La_2Ti_2O_7$ contains hypervalent La atoms within its layered perovskite structure. It is worth noting that $La_2Ti_2O_7$ exhibits efficient photocatalytic activity under the UV region, as it has a large band gap energy of approximately 3.8 eV [8−13].

Researchers are attempting to enhance the photocatalytic properties of $La_2Ti_2O_7$ in the visible light region by introducing cationic doping with transition metals. This process can extend the electronic configuration of $La_2Ti_2O_7$ towards band-edge photoresponse and narrow the band gap energy for visible light irradiation [14,15]. However, the incorporation of a single cation into a crystal structure has limitations in reducing the band gap energy due to the existence of an unoccupied impurity state. To overcome this limitation, scientists have resorted to codoping, a method that involves the simultaneous doping of two cations into the crystal structure. Codoping has been shown to enhance photocatalytic activity by maintaining charge balance, facilitating high carrier mobility, and achieving a desirable degree of band gap narrowing [16,17]. Fe and Cr codoping is a promising candidate for enhancing the photocatalytic activity of visible light driven $La_2Ti_2O_7$ through cation doping [18]. High purity $La_2Ti_2O_7$ was prepared by sol-gel method [19,20] with Fe and Cr being doped as cations during the initial preparation. Calcination was performed at different temperatures under a nitrogen atmosphere. The photocatalytic activity was analyzed using UV-Vis spectroscopy to investigate the degradation of methyl blue (MB). The synchrotron technique of Extended X-ray Absorption Fine Structure (EXAFS) was used for determine the neighbor atoms in the $La_2Ti_2O_7$ lattice structure.

2. Materials and Methods

2.1 Preparation of Photocatalytic Powder by Sol -gel Method

Photocatalytic powders ($La_2Ti_2O_7$) were prepared by sol-gel method [21] as following step. Firstly, preparation of the precursor solution by dissolve 0.476 g of titaniumbutoxide ($C_6H_{36}O_4Ti$, Sigma-Aldrich) in 31.002 g of ethylene glycol ($C_2H_6O_2$, QreC), Solution A. Solution B was prepared by dissolving 29.283 g of citric acid ($C_6H_8O_7$, Sigma- Aldrich) into 28 mL of di-water. Then solution A and B were mixed together by continuous stirring at 50 °C for 2 h to obtain solution C. Next, 0.0286 g of the iron (III) nitrate ($Fe(NO_3)_3.9H_2O$, Sigma-Aldrich), 6.1247 g of Lanthanum(III) nitrate hexahydrate ($La(NO_3)_3.6H_2O$, Sigma-Aldrich) and 0.0283 g of Chromium(III) nitrate ($Cr(NO_3)_3.9H_2O$, Sigma-Aldrich) were added into solution C and the mixture was heated to 130 °C for 8 h, resulting in the formation of a gel. The molar percent of Cr and Fe corresponding to Ti presented in the reaction are 0.005% Fe and 0.005% Cr. The calcination temperature of the obtained gel was increased gradually up to 350 °C and held for 2 h, followed by heating up to 1150 °C at a rate of 5 °C/min and holding for 2 h. In this state, the powder turned into a pale pink color, which is referred to as FeCrLTO. To investigate the effect of calcination temperature on the properties of FeCrLTO, the powder was subjected to calcination in a tube furnace under a nitrogen atmosphere (flow rate 1000 mL/min) for 24 h at different temperatures: 1150 °C (FeCrLTO1150_24h), 1250 °C (FeCrLTO1250_24h), and 1350 °C (FeCrLTO1350_24h). For comparison, control samples were calcinated at 1150 °C for 2 h under ambient atmosphere, using the same chemical composition as the experimental samples (referred to FeCrLTO1150_2h), and without the addition of Iron(III) nitrate and Chromium(III) nitrate (referred to as LTO1150_2h).

2.2 X-Ray Powder Diffraction (XRD)

The crystal structure of the synthesized photocatalysts were determined by X-ray diffraction (XRD, BRUKER D2 PHASER). The characterized conditions used for analysis are as follows: Cu-Kα radiation (λ = 1.5406 Å) at 40 kV, 40 mA, scanning range 20.70° degree (2θ) with 0.02° step size, and a counting time of 0.2 s/step. Data manipulation and XRD pattern fitting were performed using Origin Pro 2023 version 10.0.0.154 (Learning Edition)

2.3 Photocatalytic activity

The degradation of photocatalytic activity was analyzed using methylene blue (MB). The MB solution was prepared at a concentration of 1.8×10^{-4} M. For each measurement, 0.01 g of the synthesized photocatalysts powder was added to 50 mL of the MB solution [22]. The re-

action was performed in a black box with continuous stirring while exposed to LED light (EVE panel square, 18 W, Kenko L41 super pro (W) filter: light wavelength >400 nm) for a total of 180 min [23,24]. The photocatalytic activity was determined by measuring the MB degradation using UV-Vis spectroscopy (UV-Vis, model: CARY 300) equipped with a tungsten lamp as the light source. The wavelength range of the analysis was set between 300 and 700 nm. Measurement was done in a transmittance mode.

Energy band gap (E_g) was evaluated by Tauc's plot which is relative with absorbance and energy, $(\alpha hv)^2$ versus E_g. Additionally, Tauc's equation calculated E_g, shown as equation (1):

$$(\alpha hv)^2 = k(hv - E_g) \quad (1)$$

where, E_g is the optical energy gap value between the valence band and the conduction band, α is the absorption coefficient from the optical absorption spectrum using the Beer–Lambert's relation, hv is the absorption energy (h-Planck constant, v-incident frequency), k is the band tailing parameter [25].

The percentage of MB degradation was determined value of degradation, show as equation (2):

$$\%Degradation = (1 - absorbance) \times 100 \quad (2)$$

where, absorbance is the highest intensity of UV-Vis analysis at 664 nm.

2.4 X-Ray Absorption Spectroscopy (XAS)

X-ray absorption measurements were carried out at the SUT-NANOTEC-SLRI XAS beamline (BL5.2) of the Synchrotron Light Research Institute (Public Organization) (SLRI), Nakhon Ratchasima, Thailand. The synchrotron light provides electron energy of 1.2 GeV; bending magnet; beam current 80-50 mA. The beam line optics of BL5.2 is equipped with a double crystal, fixed exit, Ge (220) monochromator. The beamline possesses an energy range of 1810-3000 eV, a photon flux of 108-1010 photons/s/100mA. For Ti K-edge measurement, a Ti foil was used for energy calibration at 4966 eV on a transmission mode. For La L-edge measurement, V foil was used for energy calibration at E_0 of 5465 eV in transmission mode. Samples were measured La L-edge X-ray Absorption Near Edge Spectroscopy (XANES) and Extended X-ray Absorption Fine Structure (EXAFS) in fluorescence-mode at E_0 of 5483 eV. XANES measurements were performed in the rage of −30 eV to 80 eV of E_0, while EXAFS measurement, the photon energy scan was set up in a range of −150 eV, −10 eV, 30 , and 12k of E_0 with the photon energy step of 5 eV, 0.3 eV, and 0.05k. Samples were measured up to 4 scans. The normalized absorption data were processed after background subtraction in the pre-edge and post-edge region, then EXAFS fitting was performed using Athena and Artemis program in Demeter (version 0.9.26) Athena [26].

2.5 Field Emission Scanning Electron Microscopy (FE-SEM)

The crystal structure was analyzed by a field-emission scanning electron microscope (FE-SEM) from Carl Zeiss (model: AURIGA). The FE-SEM images revealed the shapes and pores in the crystal structure, and the analysis was performed with an acceleration voltage of 50 kV, a working distance (WD) of 6.5 mm, and a magnification of 30k. The identified elements were analyzed using energy dispersive spectroscopy (EDS).

3. Result and Discussion

The crystal phases of synthesized photocatalysts show in Figure 1 revealing that all samples exhibit the $La_2Ti_2O_7$ crystal phase as the dominant phase, and no impurities are detected (PDF 81-1066). It is apparent that the $La_2Ti_2O_7$ crystal started forming after being calcined at 1150 °C for 2 h under ambient atmosphere. The complete $La_2Ti_2O_7$ crystal was found in FeCrLTO1150_24h and FeCrLTO1250_24h, which obtained monoclinic (P1) of $La_2Ti_2O_7$. However, FeCrLTO1350_24h

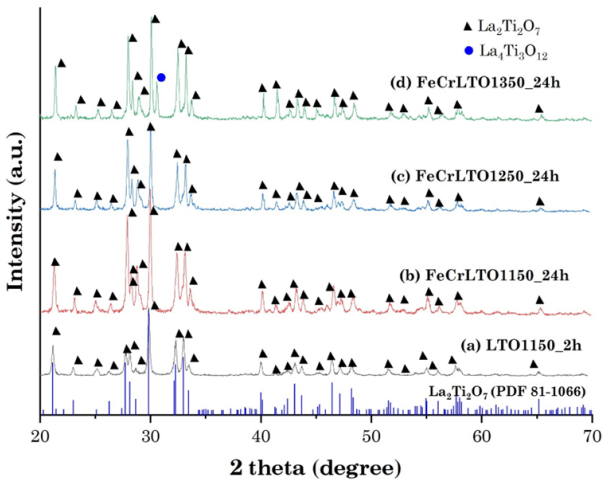

Figure 1. X-ray diffraction patterns of synthetic photocatalytic powder calcinated for 24 h under nitrogen atmosphere at different temperature; 1150 °C (a), 1250 °C (b), and 1350 °C (c).

found an extra peak of $La_4Ti_3O_{12}$ at 2θ of 30.255° (PDF 89-4520), suggesting that higher temperature induce decomposition or phase transformation from $La_2Ti_2O_7$ into mix phase of $La_2Ti_2O_7$ + $La_4Ti_3O_{12}$ [10−13]. In addition, the co-doping of Fe and Cr did not reveal any impurity phases, suggesting that the Fe and Cr cations were possibly integrated into the $La_2Ti_2O_7$ lattice [21].

The crystal morphologies of the synthesized photocatalysts were observed using FE-SEM. The sample calcined at 1150 °C (FeCr1150_24h) was found to have the smallest grain size (Figure 2(a)). As the temperature increased up to 1250 °C (FeCr1250_24h), the crystal structure became larger and the grain edges became sharper. In contrast, the sample calcined at 1350 °C (FeCr1350_24h) showed disappearing gain edges, which resulted in the large grain size connecting with the adjacent grains. The results suggest that changes in the morphology of co-doped FeCrLTO are induced

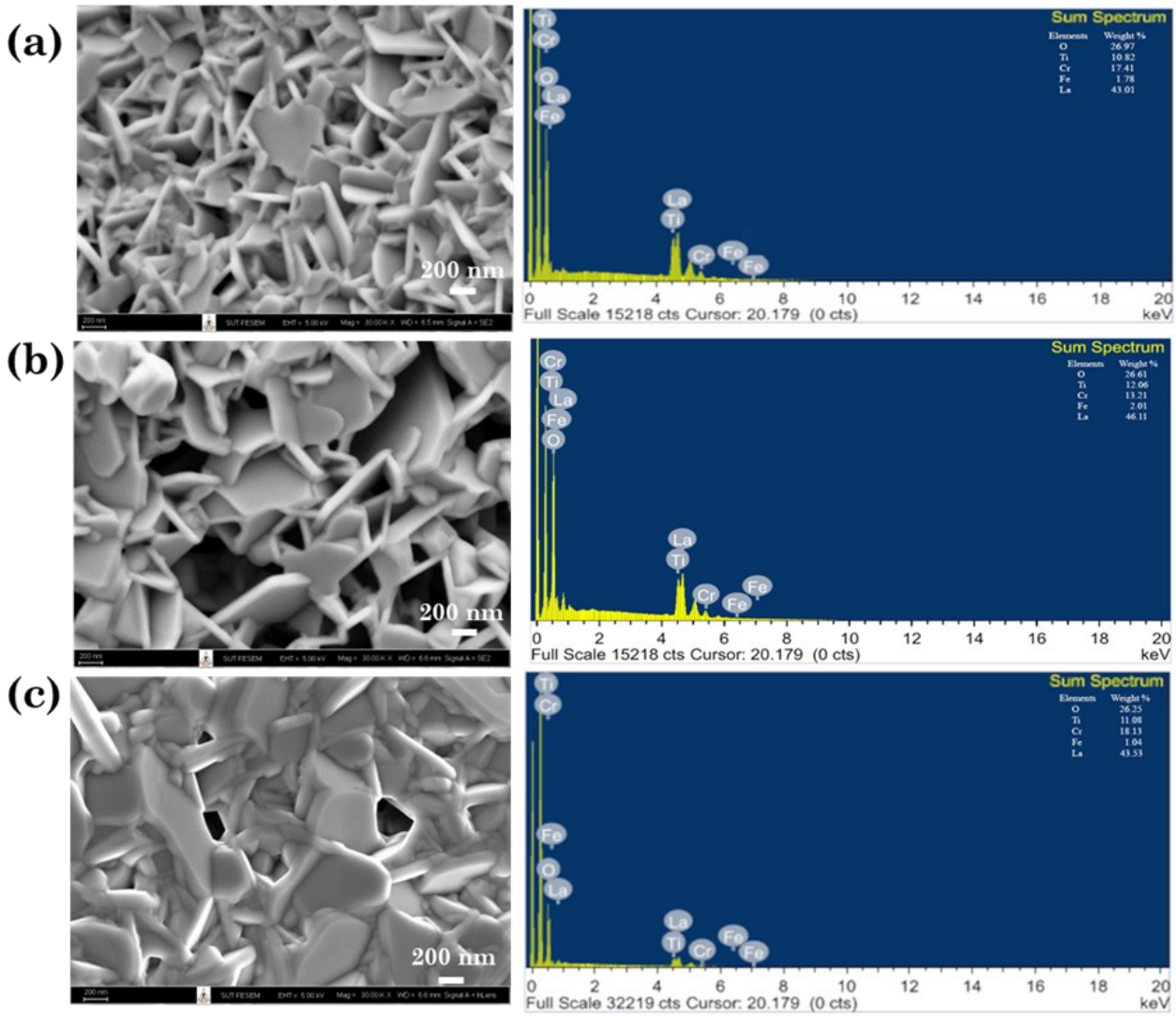

Figure 2. The FE-SEM image (left panel) and energy-dispersive X-ray (EDX) (right panel) of the synthesized photocatalysts calcined under nitrogen atmosphere for 24 h at different temperatures; 1150 °C (FeCrLTO1150_24h) (a), 1250 °C (FeCrLTO1250_24h) (b), 1350 °C (FeCrLTO1350_24h) (c).

Table 1. Elemental composition of synthesized photocatalysts examined by analyzed by FE-SEM using Energy-Dispersive X-ray (EDX) technique.

Sample	Elemental composition (% mass relative)				
	O	Ti	La	Fe	Cr
FeCr1150_24h	26.97	10.82	43.01	1.78	17.41
FeCr1250_24h	26.61	12.06	46.11	2.01	13.21
FeCr1350_24h	26.25	11.08	43.53	1.01	18.13

by the calcination temperature. Although higher temperatures are more favored for the formation of perovskite-type crystalline grains [27], but the temperature should not exceed 1250 °C to avoid adverse effects on the crystallinity.

The elemental compositions of synthesized photocatalysts were analyzed by FE-SEM using Energy-Dispersive X-ray (EDX) technique. The EDX spectra of all samples are shown in Figure 2 (right panel), and the percentage of mass relative to each element is summarized in Table 1. There was no contamination of the samples with other elements, as indicated by the peaks corresponding to O, Ti, La, Fe, and Cr. Moreover, the results confirm that Fe and Cr are incorporated into the crystal structure of $La_2Ti_2O_7$. Although the content of O and Ti was similar across all samples, there were slight variations in the contents of La, Fe, and Cr. Specifically, the FeCr1250_24h sample exhibited the highest levels of both La and Fe.

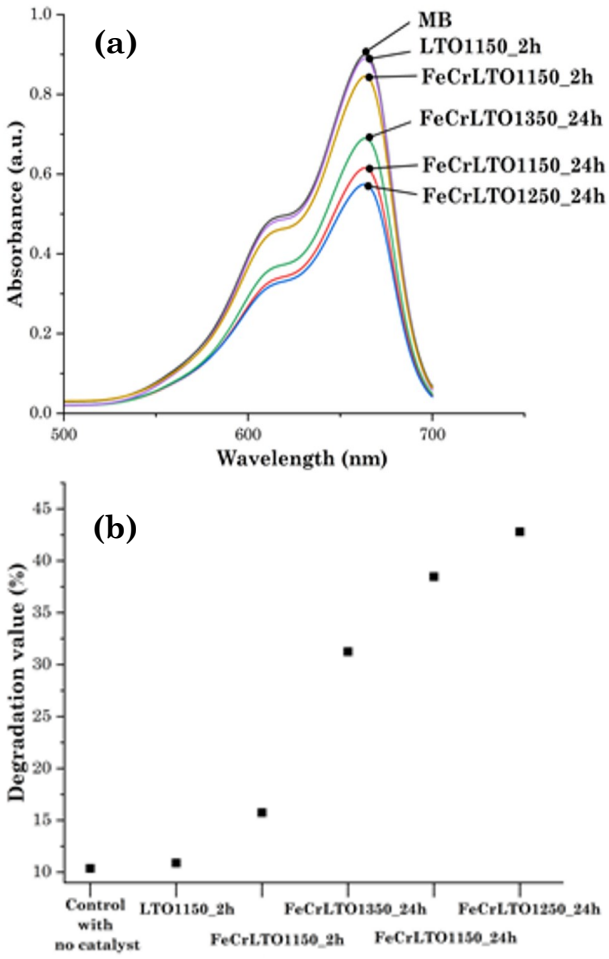

Figure 3. UV-VIS spectra of MB degradation in 180 min by synthesized photocatalysts. (a) Methylene blue degradation; (b) Degradation efficiency of catalysts.

The photocatalytic efficiency of the synthesized photocatalysts was evaluated using the MB degradation method. Visible light was irradiated onto the reaction mixture for 180min, and changes in MB concentration were monitored using UV-Vis spectroscopy at a wavelength range of 300-700 nm. The highest peak of MB can be observed clearly at 664nm. The results showed that FeCrLTO1250_24h exhibited the highest degradation efficiency, showing lower peak absorption compared to other samples. The degradation efficiency of the FeCrLTO1350_24h that underwent calcination at 1350 °C was found to be lower than that of the catalysts calcinated at other temperatures. This finding aligns with the XRD pattern observed for the FeCrLTO1350_24h photocatalyst, as shown in Figure 3(a). The effeicent dagradation of MB found that FeCrLTO1250_24h incresed upto 42.8%, which was highest dagradation of MB, for FeCrLTO1350_24h, FeCrLTO1150_24h, FeCrLTO1150_2h and LTO were 38.48%, 31.25%, 15.75% and 10.9%. In adddtion, FeCrLTO1250_24h, FeCrLTO1350_24h, FeCrLTO1150_24h were still higher efficiency than LTO and FeCrLTO1150_2h, see Figure 3(b).

Figure 4 shows Tauc's plot extrapolation used to determine the optical bandgap energy (E_g) of the synthesized photocatalysts. The FeCrLTO1250_24h photocatalyst has the lowest E_g value (2.31 eV), followed by the FeCrLTO1150_24h (2.39 eV) and FeCrLTO1350_24h (2.48 eV), respectively. According to a previous report [21], the pure $La_2Ti_2O_7$ photocatalyst

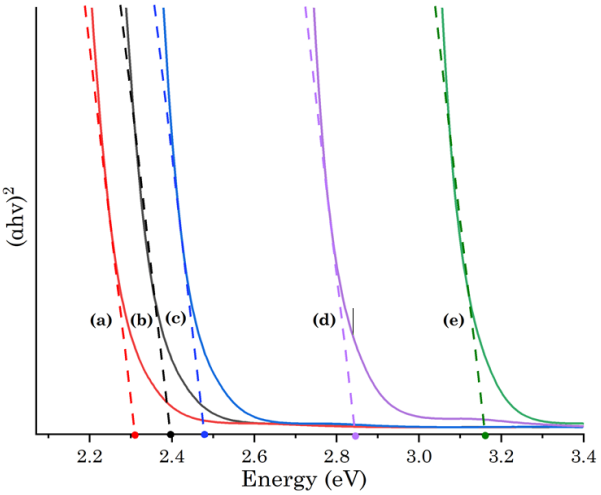

Figure 4. The optical bandgap energy (E_g) presented in Tauc's plot extrapolation of FeCrLTO1250_24h (E_g = 2.31) (a), FeCrLTO1150_24h (E_g = 2.39) (b), FeCrLTO1350_24h (E_g = 2.48) (c), FeCrLTO1150_2h (E_g = 2.84) (d), and LTO1150_2h (E_g = 3.18) (e).

has a large band gap energy of approximately 3.8 eV, which is activated by UV irradiation. The results of this study suggest that co-doping Fe and Cr into $La_2Ti_2O_7$ and calcinating the material at a high temperature under a nitrogen atmosphere for 24 h can reduce the band gap energy by more than 1 eV. This reduction in band gap energy allows the material to be activated under visible light. Additionally, previous studies have reported that the band gap energy of $La_4Ti_3O_{12}$ is 4.09 eV [28,29]. As the FeCrLTO1350_24h photocatalyst contains a mixed phase of both $La_2Ti_2O_7$ and $La_4Ti_3O_{12}$, it exhibits a higher E_g value than the other samples. Successful co-dope of Cr and Fe into photocatalyst was reported to increase catalytic activities [21,30].

XAS measurement was performed to investigate the electronic structure and local structure of synthesized $La_2Ti_2O_7$ photocatalysts. The XANES spectra of La L_3-edge of all samples show similar feature but different in terms of peak height (Figure 5). The white line (5490.82 eV) observed in the La L_3-edge spectra describes the origin of electric transition of $2p_{3/2}$ electrons to the 5p or 5d state. The strong and symmetrical white line indicates that there was no deformation of the local structure. The EXAFS k^2 weight spectra (Figure 5(b)) supported the XANES results, demonstrating a similar k^2 weight patterns. The FeCrLTO1150_2h sample had the highest white line intensity (Figure 5(b), while the FeCrLTO1250_24h and FeCrLTO1150_24h had the lowest intensity. These findings imply that the co-doping of Fe and Cr in the $La_2Ti_2O_7$ structure in different temperature can impact the p-d hybridization by modifying the local electronic structure of the surrounding oxygen atoms and transition metal ions.

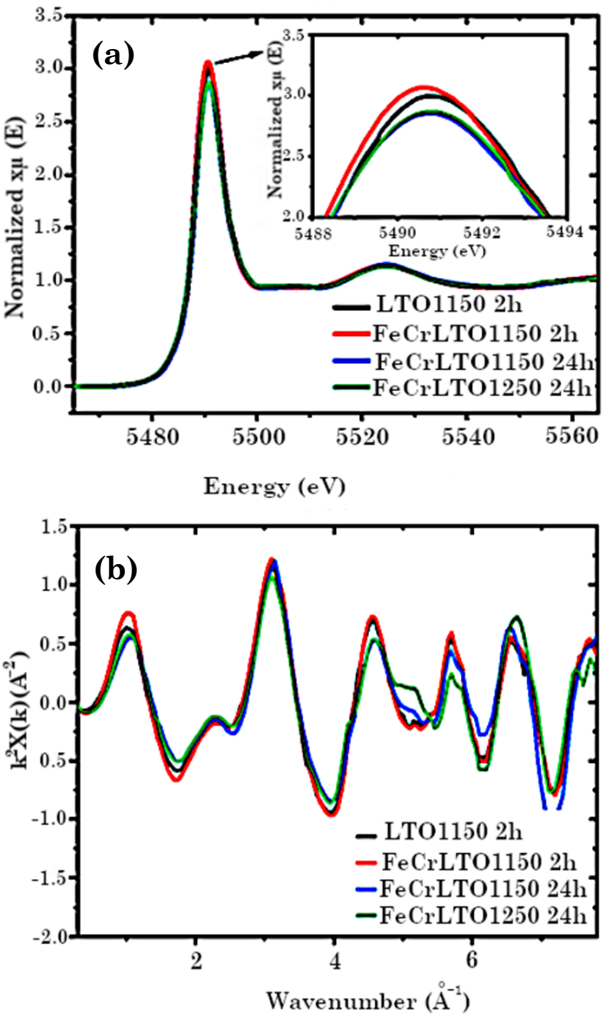

Figure 5. La L_3-edge XANES spectra of synthesized photocatalysts and the magnification of the white line region (a). The unsmoothed k^3-weighted of La L_3-edge EXAFS of synthesized photocatalysts (b).

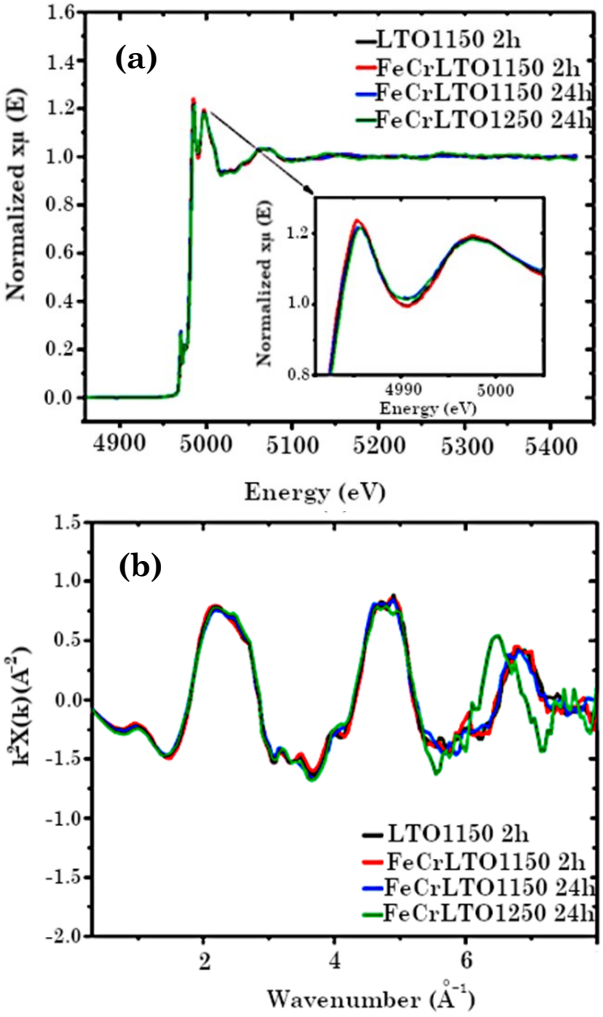

Figure 6. Ti K-edge XANES spectra of synthesized photocatalysts (a) and the magnification of the white line region. The unsmoothed k^3-weighted of Ti K-edge EXAFS of synthesized photocatalysts (b).

Ti K-edge spectrum of all synthesized $La_2Ti_2O_7$ photocatalysts show similar spectrum feature. The absorption edge position (4981.91 eV) remained unchanged, signifying that the valence state of Ti did not alter as a consequence of calcination process. The oxidation state of all samples is in the form of Ti^{4+}. All samples shared the same white line position of 4985.37 eV attributing to the 1s to 3p (or 4p) states dipole transitions. The height of this peak is generally related to the unoccupied orbital. FeCrLTO1150_2h sample showed highest intensity, which means the highest unoccupied p orbital, while FeCrLTO1250_24h had the lowest intensity. This suggests that doping Fe and Cr into $La_2Ti_2O_7$ at 1250 °C in an N_2 atmosphere may have perturbed the occupancy of the electron p orbital (Figure 6). The Ti K-edge EXAFS functions in the K space and R space of synthesized photocatalysts are mostly aligned at the same position, except FeCrLTO1250_24h which showed peak shift in k^2 weight space (Figure 6). These findings demonstrate a transformation of the local structures of Ti atoms in $FeCrLa_2Ti_2O_7$ structure.

Since the XRD patterns of the synthesized photocatalysts predominantly exhibited the $La_2Ti_2O_7$ structure, this structure was employed for the EXAFS fitting. The EXAFS best-fit parameters of LTO samples to $La_2Ti_2O_7$ were listed in Table 2. The nearest neighbour atom of Ti corresponded to the oxygen in Ti–O shells with 6 coordination. The Ti–La shells also contained 6 coordinated atoms. The R space (Figure 7) identified 3 peak positions: (Peak 1) Ti–O(1-3) (~2 Å), (Peak 2): Ti–O(4-5) (~2.3-2.5 Å), (Peak 3) Ti–La (~3.3-3.7 Å). It is noteworthy that the intensity of Peak 2 in FeCrLTO1250_24h was higher than that of Peak 3, which differed from the other samples. Therefore, EXAFS fitting cannot be wholly matched with $La_2Ti_2O_7$ structure. The extra paths of Ti–Fe and Ti–Cr were introduced to $La_2Ti_2O_7$ structure for EXAFS fitting. The perfect fitting

Table 2. The EXAFS best-fit parameters of LTO samples.

Fit parameter			LTO1150 2h	FeCrLTO1150 2h	FeCrLTO1150 24h	FeCrLTO1250 24h
R factor			0.00682	0.0080399	0.0080399	0.0081609
SO_2			0.873	0.873	0.873	0.814
Delta E_0			1.5534	0.978	0.978	2.032
R (A)	Ti–O1	N = 1	1.97097	1.98446	1.98861	2.02939
	Ti–O2	N = 1	2.14025	2.1525	2.12481	1.98773
	Ti–O3	N = 2	1.90673	1.90367	1.89527	1.94938
	Ti–O4	N = 1	2.29333	2.33259	2.33259	2.29319
	Ti–O5	N = 1	2.4969	2.53234	2.53304	2.47567
	Ti–La1	N = 1	3.42331	3.4337	3.46541	3.3569
	Ti–La2	N = 2	3.70544	3.53227	3.55604	3.73304
	Ti–La3	N = 1	3.48902	3.6486	3.6786	3.54595
	Ti–La4	N = 1	3.61854	3.43632	3.41716	3.36572
	Ti–La5	N = 1	3.3877	3.30016	3.28831	3.10888
	Ti–Fe	N=0.372	-	-	-	2.66832
	Ti–Cr	N=0.744	-	-	-	2.63988
σ2	Ti–O1	N = 1	0.00286	0.00286	0.00286	0.002
	Ti–O2	N = 1	0.00634	0.00634	0.00634	0.0634
	Ti–O3	N = 2	0.00554	0.00554	0.00554	0.00554
	Ti–O4	N = 1	0.00554	0.00554	0.00554	0.00554
	Ti–O5	N = 1	0.00443	0.00211	0.00211	0.0078
	Ti–La1	N = 1	0.00228	0.00027	0.00027	0.0034
	Ti–La2	N = 2	0.00645	0.0069	0.0069	0.00137
	Ti–La3	N = 1	0.00144	0.00645	0.00645	0.00399
	Ti–La4	N = 1	0.0069	0.00144	0.00144	0.00183
	Ti–La5	N = 1	0.00576	0.0069	0.0069	0.00003
	Ti–Fe	N=0.372	-	-	-	0.00555
	Ti–Cr	N=0.744	-	-	-	0.00842

was exhibited in the Ti–Fe degeneracy of 0.372 and Ti–Cr degeneracy of 0.744. The interatomic distance of Ti–Fe and Ti–Cr are 2.67 Å and 2.64 Å, respectively. The evidence implied that the substituted Fe and Cr atom was positioned adjacent to the Ti atom in $La_2Ti_2O_7$ structure but not the La atom. In $La_2Ti_2O_7$, the Ti atom acts as the photoactive center, absorbing photons and promoting electrons to higher energy levels. The presence of substituted Fe and Cr atoms adjacent to the Ti atom can induce electron transfer from these metal atoms to the Ti atom, thus facilitating the separation of electron-hole pairs and improving the photocatalytic efficiency.

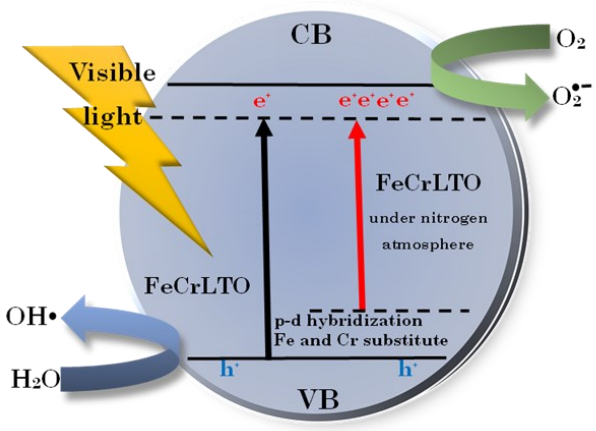

Scheme 1. Model of photocatalytic activities of synthesized FeCrLTO and FeCrLTO under nitrogen atmosphere for waste water treatment.

The substituted doping of Cr and Fe in the $La_2Ti_2O_7$ structure can affect the *p-d* hybridization between the oxygen 2p orbitals and the transition metal 3d orbitals, as indicated by the XANES results. The 3d orbitals of Cr and Fe have partially filled electrons that can interact with the 2p orbitals of the surrounding oxygen atoms, leading to hybridization between these orbitals. This interaction can then cause changes in the electronic structure of the nearby oxygen atoms and Ti ions, ultimately affecting the *p-d* hybridization. Therefore, substituted doping of Cr and Fe in the $La_2Ti_2O_7$ struc-

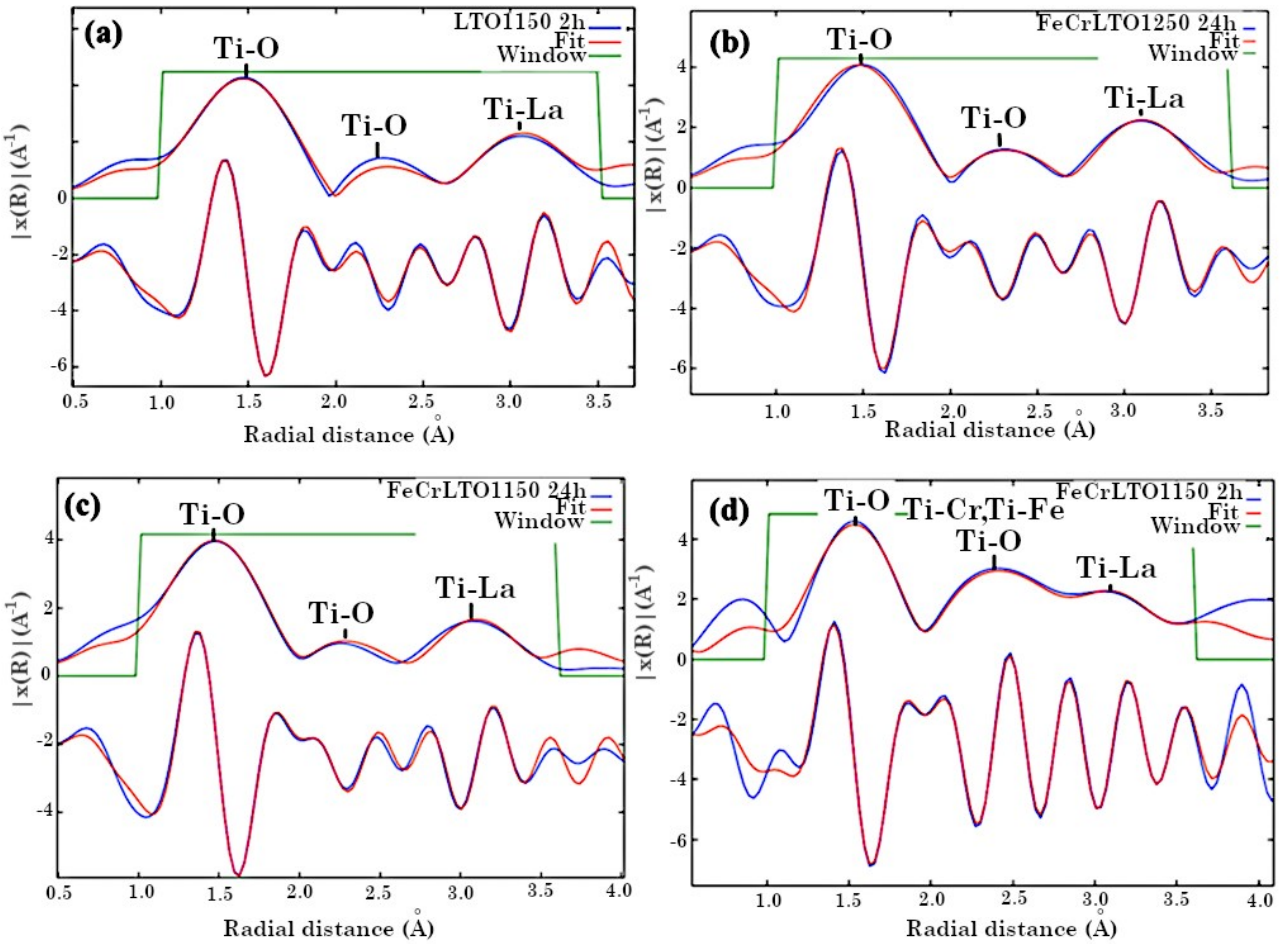

Figure 7. Ti K-edge EXAFS of synthesized photocatalysts with fits taken from the $La_2Ti_2O_7$ model. (a) LTO1150_2h, (b) FeCrLTO1150_2h, (c) FeCrLTO1150_24h, (d) FeCrLTO1250_24h. Upper graph is the k^3-weighted EXAFS. Lower graph is the Fourier transforms of the EXAFS signals in R space. Phase shifts were not corrected.

ture can lead to changes in their optical and photocatalytic properties (Scheme 1). These changes reduce the band gap of the photocatalysts, causing their absorption spectrum to shift and ultimately improve their photocatalytic performance. Extensive research has been conducted on the use of orbital hybridization to regulate the electronic structures and surface chemisorption properties of transition metals in order to enhance the performance of catalysts [31]. Moreover, calcination under a N_2 atmosphere can be used to control the oxygen content of the material and to prevent oxidation or reduction reactions that could alter the electronic properties of (Fe,Cr) co-doping $La_2Ti_2O_7$.

4. Conclusion

The sol-gel method is appropriate preparation for $La_2Ti_2O_7$-based photocatalysts that can be activated by visible light, the optimal approach with co-doping of Fe and Cr at the concentration of 0.005 molar percent corresponding to Ti atom. The calcination process was carried out under an N_2 atmosphere to control the oxygen concentration of the material and prevent the oxidation and reduction reactions that could modify the electronic characteristics of the (Fe,Cr) co-doped $La_2Ti_2O_7$. The heating temperature of 1250 °C for 24 h was provided the best photocatalytic efficiency. Fe and Cr was found to be substituted into the lattice sites of the photocatalysts. The Fe and Cr substitution leads to the transfer of electrons from Fe and Cr metal atoms to the Ti atom, thus facilitating the separation of electron-hole pairs and improving the photocatalytic efficiency. Additionally, Fe and Cr alter the p-d hybridization within the $La_2Ti_2O_7$ lattice, resulting in a reduction of the band gap and the absorption of lower energy.

Acknowledgments

The authors of the present work would like to extend their heartfelt gratitude to all those who have supported and contributed to this research endeavor. Firstly, the authors would like to acknowledge Suranaree University of Technology for their generous financial support, which was essential in bringing this project to fruition. The authors are also deeply appreciative of Asst. Prof. Dr. Sukasem Watcharamaisakul, who provided invaluable guidance and mentorship throughout the course of this research. Their expertise and support were instrumental in the success of this work. Finally, the authors would like to express their sincere gratitude to Dr. Waraporn Tanthanuch and Dr. Ratchadaporn Supruangnet for their valuable contributions and support, sharing their idea, XAS experimental plan and measurement, and data analysis. Their contributions were critical to the progress and quality of this work.

CRedit Author Statement

Authors contributions are as follows. Sukasem Watcharamaisakul conceived conceptualization and planned the experiments, review and editing the manuscript. Hussanai Luangthsanarak, author, performed methodology, formal analysis, investigation, validation and writing- original draft. Waraporn Tanthanuch and Ratchadaporn Supruangnet contributed for the XAS experimental plan, measurement, data analysis and draft the manuscript on XAS part. Ratchadaporn Supruangnet contributed on experimental plan and revised the manuscript.

References

[1] Nakata, K., Fujishima, A. (2012). TiO_2 photocatalysis: Design and applications. *Journal of Photochemistry and Photobiology C: Photochemistry Reviews*, 13, 169-189. DOI: 10.1016/j.jphotochemrev.2012.06.001.

[2] Shaham-Waldmann, N., Paz, Y. (2016). Away from TiO_2: A critical minireview on the developing of new photocatalysts for degradation of contaminants in water. *Materials Science in Semiconductor Processing*, 42, 72-80. DOI: 10.1016/j.mssp.2015.06.068.

[3] Spasiano, D., Marotta, R., Malato, S., Fernandez-Ibañez, P., Di Somma, I. (2015). Solar photocatalysis: Materials, reactors, some commercial, and pre-industrialized applications. A comprehensive approach. *Applied Catalysis B: Environmental*, 170-171, 90-123. DOI: 10.1016/j.apcatb.2014.12.050.

[4] Banerjee, S., Dionysiou, D.D., Pillai, S.C. (2015). Self-cleaning applications of TiO_2 by photo-induced hydrophilicity and photocatalysis. *Applied Catalysis B: Environmental*, 176-177, 396-428. DOI: 10.1016/j.apcatb.2015.03.058.

[5] Gerischer, H., Heller, A. (1991). The role of oxygen in photooxidation of organic molecules on semiconductor particles. *The Journal of Physical Chemistry*, 95(13), 5261-5267. DOI: 10.1021/j100166a063.

[6] Shemer, G., Paz, Y. (2011). Interdigitated Electrophotocatalytic Cell for Water Purification. *International Journal of Photoenergy*, 2011, 596710. DOI: 10.1155/2011/596710.

[7] Batzill, M. (2011). Fundamental aspects of surface engineering of transition metal oxide photocatalysts. *Energy & Environmental Science*, 4(9), 3275-3286. DOI: 10.1039/C1EE01577J.

[8] Hwang, D.W., Cha, K.Y., Kim, J., Kim, H.G., Bae, S.W., Lee, J.S. (2003). Photocatalytic Degradation of CH_3Cl over a Nickel-Loaded Layered Perovskite. *Industrial & Engineering Chemistry Research*, 42(6), 1184-1189. DOI: 10.1021/ie020457c.

[9] Hwang, D.W., Kim, H.G., Kim, J., Cha, K.Y., Kim, Y.G., Lee, J.S. (2000). Photocatalytic Water Splitting over Highly Donor-Doped (110) Layered Perovskites. *Journal of Catalysis*, 193(1), 40-48. DOI: 10.1006/jcat.2000.2875.

[10] Kim, J., Hwang, D.W., Kim, H.-G., Bae, S.W., Ji, S.M., Lee, J.S. (2002). Nickel-loaded $La_2Ti_2O_7$ as a bifunctional photocatalyst. *Chemical Communications,* (21), 2488-2489. DOI: 10.1039/B208092C.

[11] Ku, Y., Wang, L.C., Ma, C.M. (2007). Photocatalytic Oxidation of Isopropanol in Aqueous Solution Using Perovskite-Structured $La_2Ti_2O_7$. *Chemical Engineering & Technology*, 30(7), 895-900. DOI: 10.1002/ceat.200700071.

[12] Wang, R., Xu, D., Liu, J., Li, K., Wang, H. (2011). Preparation and photocatalytic properties of $CdS/La_2Ti_2O_7$ nanocomposites under visible light. *Chemical Engineering Journal*, 168(1), 455-460. DOI: 10.1016/j.cej.2011.01.035.

[13] Wang, Q., An, N., Chen, W., Wang, R., Wang, F., Lei, Z., Shangguan, W. (2012). Photocatalytic water splitting into hydrogen and research on synergistic of Bi/Sm with solid solution of Bi-Sm-V photocatalyst. *International Journal of Hydrogen Energy*, 37(17), 12886-12892. DOI: 10.1016/j.ijhydene.2012.05.080.

[14] Borgarello, E., Kiwi, J., Graetzel, M., Pelizzetti, E., Visca, M. (1982). Visible light induced water cleavage in colloidal solutions of chromium-doped titanium dioxide particles. *Journal of the American Chemical Society*, 104(11), 2996-3002. DOI: 10.1021/ja00375a010.

[15] Lin, L., Chai, Y., Yang, Y., Wang, X., He, D., Tang, Q., Ghoshroy, S. (2013). Hierarchical Gd-La codoped TiO_2 microspheres as robust photocatalysts. *International Journal of Hydrogen Energy*, 38(6), 2634-2640. DOI: 10.1016/j.ijhydene.2012.11.100.

[16] Lin, Y., Jiang, Z., Zhu, C., Hu, X., Zhu, H., Zhang, X., Fan, J., Lin, S.H. (2013). The optical absorption and hydrogen production by water splitting of (Si,Fe)-codoped anatase TiO_2 photocatalyst. *International Journal of Hydrogen Energy*, 38(13), 5209-5214. DOI: 10.1016/j.ijhydene.2013.02.079.

[17] Long, R., English, N.J. (2011). Band gap engineering of double-cation-impurity-doped anatase-titania for visible-light photocatalysts: a hybrid density functional theory approach. *Physical Chemistry Chemical Physics*, 13(30), 13698-13703. DOI: 10.1039/C1CP21454C.

[18] Zhang, J., Tse, K., Wong, M., Zhang, Y., Zhu, J. (2016). A brief review of co-doping. *Frontiers of Physics*, 11(6), 117405. DOI: 10.1007/s11467-016-0577-2.

[19] Sharma, M., Pathak, M., Kapoor, P.N. (2018). The sol-gel method: pathway to ultrapure and homogeneous mixed metal oxide nanoparticles. *Asian Journal of Chemistry*, 30(7), 1405-1412. DOI: 10.14233/ajchem.2018.20845.

[20] Venkatachalam, N., Palanichamy, M., Murugesan, V. (2007). Sol-gel preparation and characterization of nanosize TiO_2: Its photocatalytic performance. *Materials Chemistry and Physics*, 104(2-3), 454-459. DOI: 10.1016/j.matchemphys.2007.04.003.

[21] Hu, S., Jia, L., Chi, B., Pu, J., Jian, L. (2014). Visible light driven (Fe,Cr)-codoped $La_2Ti_2O_7$ photocatalyst for efficient photocatalytic hydrogen production. *Journal of Power Sources*, 266, 304-312. DOI: 10.1016/j.jpowsour.2014.05.054.

[22] Jin, M., Nagaoka, Y., Nishi, K., Ogawa, K., Nagahata, S., Horikawa, T., Katoh, M., Hayashi, J. (2008). Adsorption properties and photocatalytic activity of TiO_2 and La-doped TiO_2. *Adsorption*, 14(2), 257-263. DOI: 10.1007/s10450-007-9095-4

[23] Turon, V., Anxionnaz-Minvielle, Z., Willison, J.C. (2018). Replacing incandescent lamps with an LED panel for hydrogen production by photofermentation: Visible and NIR wavelength requirements. *International Journal of Hydrogen Energy*, 43(16), 7784-7794. DOI: 10.1016/j.ijhydene.2018.03.019.

[24] Claypool, N.B., Lieth, J.H. (2020). Physiological responses of pepper seedlings to various ratios of blue, green, and red light using LED lamps. *Scientia Horticulturae*, 268, 109371. DOI: 10.1016/j.scienta.2020.109371.

[25] Etacheri, V., Geiger, U., Gofer, Y., Roberts, G. A., Stefan, I.C., Fasching, R., Aurbach, D. (2012). Exceptional Electrochemical Performance of Si-Nanowires in 1,3-Dioxolane Solutions: A Surface Chemical Investigation. *Langmuir*, 28(14), 6175-6184. DOI: 10.1021/la300306v.

[26] Ravel, B., Newville, M., (2005). ATHENA, ARTEMIS, HEPHAESTUS: data analysis for X-ray absorption spectroscopy using IFEFFIT. *Journal of Synchrotron Radiation,* 12, 537-541. DOI: 10.1107/S0909049505012719.

[27] Pillai, S.C., Periyat, P., George, R., McCormack, D.E., Seery, M.K., Hayden, H., Colreavy, J., Corr, D., Hinder, S.J. (2007). Synthesis of High-Temperature Stable Anatase TiO_2 Photocatalyst. *The Journal of Physical Chemistry C*, 111(4), 1605-1611. DOI: 10.1021/jp065933h.

[28] Ma, Z., Wu, K., Sa, R., Li, Q., He, C., Yi, Z. (2015). Mechanism of enhanced photocatalytic activities on N-doped $La_2Ti_2O_7$: An insight from density-functional calculations. *International Journal of Hydrogen Energy*, 40(2), 980-989. DOI: 10.1016/j.ijhydene.2014.11.088.

[29] Low, J., Yu, J., Jaroniec, M., Wageh, S., Al-Ghamdi, A.A. (2017). Heterojunction Photocatalysts. *Advanved Materials*, 29(20), 1601694. DOI: 10.1002/adma.201601694.

[30] Lin, N., Gong, Y., Wang, R., Wang, Y., Zhang, X. (2022). Critical review of perovskite-based materials in advanced oxidation system for wastewater treatment: Design, applications and mechanisms. *Journal of Hazardous Materials*, 424, 127637. DOI: 10.1016/j.jhazmat.2021.127637.

[31] Chen, H., Wu, Q., Wang, Y., Zhao, Q., Ai, X., Shen, Y., Zou, X. (2022). d–sp orbital hybridization: a strategy for activity improvement of transition metal catalysts. *Chemical Communications*, 58(56), 7730-7740. DOI: 10.1039/D2CC02299K.